Elasticity and rheology of platinum under high pressure and nonhydrostatic stress

Abby Kavner* and Thomas S. Duffy
Department of Geosciences, Princeton University, Princeton, New Jersey 08544, USA
(Received 24 October 2003; revised manuscript received 9 July 2003; published 6 October 2003)

Using radial x-ray diffraction under nonhydrostatic compression in a diamond-anvil cell, we determine a lower bound of the yield strength of polycrystalline platinum to be 2.2 to 3.3 GPa in the pressure range of 4.2 to 22.4 GPa at room temperature. The elastic anisotropy $S=2(S_{11}-S_{12})/S_{44}$ of platinum is also evaluated, and is equal to 1.47(16) throughout this pressure range. In addition, platinum shows a time-dependent relaxation under nonhydrostatic stress at both ambient temperatures and, in a separate set of experiments, during laser heating. Average strain rates measured for platinum are 10^{-7} s^{-1} at 300 K and 10^{-5} s^{-1} at 1200 K, resulting in effective creep viscosities of 10^{15} Pa s at 300 K and 10^{13} Pa s at 1200(300) K.

DOI: 10.1103/PhysRevB.68.144101 PACS number(s): 62.50.+p, 62.40.+i, 62.20.Dc, 62.20.Hg

INTRODUCTION

Measuring material elasticity and rheology at high pressures is important for a variety of scientific and technological applications including the physics of planetary interiors,[1,2] and the design and modeling of dynamic compression experiments.[3] In addition, understanding a material's behavior at its elastic limit provides fundamental insight into the physics of solid structure, atomic bonding, and defect microdynamics.[4] Rheological properties of materials under high pressure such as yield point, hardness, and toughness are even less well constrained by theory and experiment, in part because these properties are often dependent on sample preparation and history effects, such as cold rolling, annealing, and strain rate during deformation.[5]

Experimental measurements of elastic tensors of metals have mostly been limited to moderate pressures ($<\sim 2$ GPa).[6] Elasticity of metals at ultrahigh pressures is thus a relatively unexplored regime, although there are a few first-principles calculations of the high *P, T* elasticity of materials such as Fe.[7] To test models of ultrahigh pressure behavior there is a need to extend elastic measurements into this regime.

Platinum is important as a pressure standard owing to its chemical and mechanical stability. In addition, platinum's ability to absorb infrared radiation makes it a commonly used laser absorber and internal pressure standard in laser-heated diamond cell experiments designed to measure high-pressure high-temperature phase stability and equations of state.[8,9] Therefore, a thorough understanding of platinum's high pressure strength and elastic behavior is required to interpret experimental measurements from the laser-heated diamond cell. For example, uncertainty in the location of the ringwoodite-perovskite+oxide transition in Mg_2SiO_4 is thought to be due to uncertainties in the $P(V,T)$ equation of state of standards such as Au and Pt.[10] The use of platinum as a standard is hindered by the fact that there is only a partial set of experimental values of the elastic compliance tensor as a function of pressure.[11] Here we investigate both plastic rheology and elastic anisotropy of platinum subjected to large, nonhydrostatic stresses in the diamond anvil cell using radial x-ray diffraction techniques.[12,13]

EXPERIMENTAL PROCEDURE

In the first of two experiments, pure platinum powder (*Aldrich, 99.99%, grain size* ~ 1 μm) was precompressed between two diamonds to form a $\sim$20-μm-thick foil. A $\sim 50\times 50$ μm^2 piece of Pt foil was loaded in a diamond-anvil cell equipped with a beryllium gasket with a 100-μm diameter sample chamber. In a second experiment, a smaller ($20\times 20\times 10$ μm^3) piece of platinum foil was placed atop a larger chip ($\sim 75\times 75\times 20$ μm^3) of polycrystalline cubic $(Mg,Fe)_2SiO_4$ ringwoodite within the same sized sample chamber. In both cases, no pressure transmitting medium was used, as the goal of the experiment was to create a nonhydrostatic sample environment.

Energy-dispersive x-ray diffraction experiments were performed at the X17C beamline of the National Synchrotron Light Source. In the geometry for radial diffraction, the x-ray beam (7 $\mu m\times 14$ μm) passes through the beryllium gasket and the sample between the diamond faces.[13] The first experiment consisted of four pressure steps, and the second consisted of seven pressure steps. At each pressure step, a series of 5 to 12 diffraction patterns were obtained by rotating the diamond cell about the x-ray beam. Before each diffraction pattern was obtained, the cell was scanned in the horizontal and vertical directions to ensure that the central part of the sample was always centered within the x-ray beam. Each diffraction pattern was collected at a fixed 2θ angle for periods ranging from 5 min to 5 h, with most patterns collected for $\sim$10 min. The solid-state Ge detector was calibrated with a series of fluorescence standards, and the 2θ angles (which ranged from 8 to 12) were calibrated using a gold foil. The radial diffraction geometry and analysis methods are described in detail in several papers[12,14–18] and shown in Fig. 1.

Model. The elastic behavior of a cubic material loaded in the diamond cell under a nonhydrostatic state of stress is described by Singh[12] and briefly summarized here. The stress is assumed to be biaxial, with the maximum principal stress σ_1 in the diamond loading direction, and the cylindrically symmetric minimum principal stress σ_3 in the plane of the gasket. Under constant stress conditions (Reuss bound), the lattice strain of a polycrystalline aggregate of cubic material is

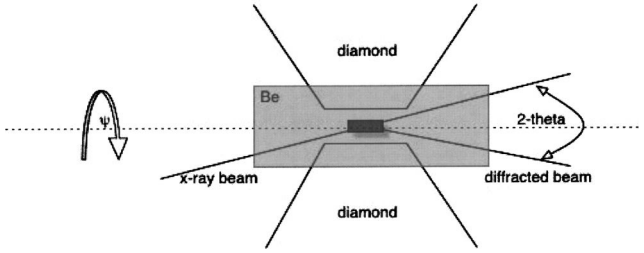

FIG. 1. Geometry of radial diffraction experiment. Polycrystalline sample (dark gray) is enclosed in a beryllium gasket between two diamonds. The cell is rotated (ψ) about the axis depicted by the dotted line. The relationship between the incoming x-ray beam and the diffracted beam remains fixed.

$$\Delta\varepsilon_{(hkl)} = \varepsilon_{(hkl)} - \varepsilon_{\text{hydro}} = (t/3)[S_{11} - S_{12} - 3S\Gamma(khl)](1 - 3\cos^2\psi), \quad (1)$$

where $\varepsilon(hkl)$ are the measured lattice strains; $\varepsilon_{\text{hydro}}$ the hydrostatic component of the strain; t the differential stress $(\sigma_1 - \sigma_3)$; *Sij*'s the single-crystal elastic compliances; $S = S_{11} - S_{12} - 0.5S_{44}$ a measure of the elastic anisotropy; Γ an orientation factor given by $(h^2k^2 + k^2l^2 + h^2l^2)/(h^2 + k^2 + l^2)^2$, where *h, k,* and *l* are the Miller indices of the reflecting plane; and ψ the angle between the diffracting plane normal and the diamond cell axis (assumed to be the maximum principal stress).

At $\psi = 90°$, the strains determined from the (111) ($\Gamma_{\max} = 0.333$) and (200) ($\Gamma_{\min} = 0$) lines through Eq. (1) are given by

$$\Delta\varepsilon^{90°}_{(111)} = \varepsilon^{90°}_{(111)} - \varepsilon_{\text{hydro}} = (t/6)(S_{44}) \quad (2)$$

and

$$\Delta\varepsilon^{90°}_{(200)} = \varepsilon^{90°}_{(200)} - \varepsilon_{\text{hydro}} = (t/3)(S_{11} - S_{12}), \quad (3)$$

where $\Delta\varepsilon_{(hkl)}$ is the difference between the lattice strain at 90° and the hydrostatic value of the strain, defined by $1 - 3\cos^2\psi = 0$ (where $\psi = 54.7$). $\varepsilon_{(111)} = \varepsilon_{(200)}$ for an elastically isotropic material.

Under the Voigt bound (constant strain), the angular dependence of the strain is not a function of (hkl), and is equal to

$$\langle\varepsilon_{(khl)}\rangle - \varepsilon_{\text{hydro}} = (t/3)(1/G_v)(1 - 3\cos^2\psi), \quad (4)$$

where G_v is the Voigt (constant strain) bound on the shear modulus. The Voigt strain values as a function of ψ fall between the bounds generated by Eqs. (2) and (3). For an elastically isotropic material, Eqs. (2), (3), and (4) yield identical results.

EXPERIMENTAL RESULTS

Angle dependence of lattice parameters. Diffraction patterns (Fig. 1) were indexed, and *d*-spacings and lattice parameters were calculated from the energy of each peak. The Eulerian strain $(\varepsilon = 1/2[(V/V_0)^{2/3} - 1])$ was calculated for each individual peak, using $V_0 = 60.3$ Å^3 (Table I). In the initial experiment, the first two data sets were obtained on compression, the third on decompression, and the final one on recompression. In the second set, the behavior of platinum was investigated under compression only. At pressures below 3 GPa (e.g., experiments PtP1 and PtP2) strain is approximately constant as ψ changes. As pressure is increased, the strain shows an increasing ψ dependence. For example, diffraction patterns obtained for platinum at 13.4 GPa (Fig. 2) show that the (200) peak shifts by over 500 eV between the maximum ($\psi = 0°$) and minimum ($\psi = 90°$) stress directions. The magnitude of this strain difference is 0.0237, almost twice as large as the hydrostatic component of the strain (0.0150). This angle dependent strain is roughly five times what gold experiences during similar compression experiments[15,16] and is comparable to results for rhenium.[16] Translated into pressure, the difference between the compression at 0° and 90° is significant; at 4.2 GPa the apparent pressures obtained using different (hkl) and ψ values are $P^{0°}_{(111)} = 4.7$ GPa and $P(111)^{90°} = 1.1$ GPa. $P(200)^{90°} = -1.4$ GPa. This last demonstrates both the extreme change of lattice strain with ψ, to the point where it indicates an expansion of lattice planes normal to the loading axis under modest pressures, and the lattice-plane dependence of the response indicating platinum's anisotropic nature. For comparison, sources of error corresponding to angle calibration and detector energy calibration may affect the peak positions by ~1 and ~100 eV, equivalent to 0.01 and 1 GPa, respectively. However, neither of these sources of possible systematic error contributes a ψ dependence, so contributes errors neither to the strength nor to the anisotropy measurement.

Data analysis. At each pressure step the angular dependence of the lattice strain was measured by separately fitting the lattice strain for each (hkl) versus $1 - 3\cos^2\psi$ (Fig. 3). For each lattice plane at a given compression, the fits generate three independent parameters: the hydrostatic value of the strain, the amplitude of the ψ dependence, and an angular offset representing the orientation relationship between the diamond cell axis and the principal axes of the strain tensor (Table II). This angular offset provides a test of a key assumption: that the principal stress axes are aligned with the diamond cell axis. If the lattice strains are plotted as a straight line (vs $1 - 3\cos^2\psi$ instead of vs ψ) a potential means of testing this assumption is lost, and only two independent parameters are measured: the hydrostatic value and the amplitude of the ψ dependence.

Through the lattice strain fits, the complete data set at a given compression provides three independent pieces of information: (i) the hydrostatic lattice strain given by the $\langle\varepsilon_{(hkl)}\rangle$ at $\psi = 54.7°$ (see above); (ii) $\varepsilon^{\text{amp}}_{(200)}$, the strain amplitude at $\Gamma = 0$ (minimum value); and (iii) $\varepsilon^{\text{amp}}_{(111)}$, the strain amplitude at $\Gamma = 0.333$ (maximum value) (Table II). Taken together, these last two comprise the isotropic response—the extent to which all of the diffraction lines respond to a deviatoric stress—and an anisotropic response—how each line responds slightly differently to the applied stress, depending on its Γ value. At each compression step, these three parameters yield the pressure, the magnitude of the elastically supported shear stress, and a single constraint on the elastic

TABLE I. Strain as a function of *hkl* and rotation angle, calculated for each pressure step in the two radial diffraction experiments. Data is shown in time-order. See Table II for summary data.

	angle	$\varepsilon(111)$	$\varepsilon(200)$	$\varepsilon(220)$	$\varepsilon(311)$	$\varepsilon(222)$	$\varepsilon(400)$	$\varepsilon(331)$	$\varepsilon(422)$
1st Pt20									
	0	−0.0258							
	180	−0.0244							
	160	−0.0254							
	180	−0.0246							
	160	−0.0226							
	140	−0.0194							
	0	−0.0273							
	60	−0.0142							
	70	−0.0130	−0.0107	−0.0137					
	80	−0.0138	−0.0123	−0.0138					
	90	−0.0106	−0.0090	−0.0111					
	90	−0.0120	−0.0108	−0.0129					
1st pt30	0	−0.0336							
	90	−0.0160							
	70	−0.0190							
	110	−0.0171							
	180	−0.0299							
	165	−0.0301							
	195	−0.0318							
	270	−0.0152							
	340	−0.0309							
	20	−0.0298							
	0	−0.0301							
	90	−0.0159							
1st Low B	0	−0.0144	−0.0177	−0.0168					
	180	−0.0143	−0.0161	−0.0158					
	90	−0.0013	0.0013	−0.0023					
	20	−0.0133	−0.0157	−0.0151					
	340	−0.0098	−0.0127	−0.0113					
	270	−0.0004	0.0022	−0.0009					
	290	−0.0009	0.0018	−0.0002					
	250	−0.0059	−0.0028	−0.0066					
	0	−0.0123	−0.0149						
1st Pt10	0	−0.0165	−0.0162	−0.0192					
	180	−0.0168	−0.0199	−0.0179					
	90	−0.0029	0.0020	−0.0033					
	20	−0.0178	−0.0197						
	340	−0.0121	−0.0121						
2nd PtP1	0	−0.0013	0.0000	−0.0015					
	20	−0.0010	0.0003	−0.0015					
	40	−0.0005	0.0005	−0.0008					
	60	−0.0005	0.0008	−0.0010					
	90	−0.0005	0.0005	−0.0010					
2nd PtP2	90	−0.0033	−0.0018	−0.0036					
	70	−0.0028	−0.0010	−0.0036					
	50	−0.0033	−0.0015	−0.0038					
	30	−0.0053	−0.0038	−0.0053					
	0	−0.0064	−0.0051	−0.0064					
2nd PtP3									
	−20	−0.0187	−0.0217	−0.0192					
	10	−0.0197	−0.0234	−0.0197					

TABLE I. (*Continued*).

	30	−0.0172	−0.0192	−0.0177				
	50	−0.0134	−0.0132	−0.0144				
	70	−0.0069	−0.0038	−0.0074				
	90	−0.0048	−0.0013	−0.0043				
	110	−0.0069	−0.0036	−0.0069				
	0	−0.0197	−0.0227	−0.0194				
	0	−0.0179	−0.0199	−0.0177				
	0	−0.0174	−0.0194	−0.0172				
2nd PtP4	90	−0.0074	−0.0043	−0.0071				
	110	−0.0094	−0.0058	−0.0094				
	70	−0.0122	−0.0099	−0.0129				
	50	−0.0174	−0.0177	−0.0179				
	40	−0.0202		−0.0204				
	30	−0.0207	−0.0234	−0.0212				
	10	−0.0239	−0.0286	−0.0244				
	0	−0.0237	−0.0279	−0.0237				
2nd PtP5	90	−0.0104	−0.0069	−0.0096	−0.0079	−0.0081	−0.0064	−0.0114	−0.0106
	110	−0.0117	−0.0081	−0.0109	−0.0094	−0.0089	−0.0081	−0.0127	−0.0124
	70	−0.0129	−0.0096	−0.0134	−0.0119	−0.0106	−0.0101	−0.0149	−0.0127
	50	−0.0207	−0.0214	−0.0214	−0.0199	−0.0182	−0.0212	−0.0197	−0.0179
	30	−0.0239	−0.0274	−0.0249	−0.0254	−0.0232	−0.0281	−0.0244	−0.0237
	10								
	0	−0.0244	−0.0286	−0.0262	−0.0272	−0.0239	−0.0296	−0.0249	−0.0244
	−20	−0.0219	−0.0247	−0.0234	−0.0237	−0.0207	−0.0247	−0.0227	−0.0222
2nd PtP6	−20	−0.0254	−0.0299	−0.0294	−0.0301	−0.0269	−0.0338		
	−40	−0.0197	−0.0202	−0.0227	−0.0214	−0.0194	−0.0207		
	90	−0.0129	−0.0099	−0.0124	−0.0109	−0.0112	−0.0099	−0.0134	−0.0129
	110	−0.0149	−0.0109	−0.0137	−0.0122	−0.0117	−0.0114	−0.0144	−0.0142
	130	−0.0192	−0.0174	−0.0197	−0.0182	−0.0162	−0.0184	−0.0192	−0.0187
	150	−0.0232	−0.0242	−0.0249	−0.0232	−0.0217	−0.0249	−0.0229	−0.0212
	170	−0.0309	−0.0370	−0.0301	−0.0316	−0.0281	−0.0346	−0.0274	
	180	−0.0291	−0.0338	−0.0296	−0.0306	−0.0274	−0.0336		
	200	−0.0276	−0.0306	−0.0284	−0.0284	−0.0259	−0.0311		
2nd PtP7	20	−0.0309	−0.0353	−0.0321	−0.0321	−0.0296			
	40	−0.0279	−0.0294	−0.0286	−0.0284	−0.0286			
	20	−0.0301	−0.0328	−0.0314	−0.0318	−0.0289			
	90	−0.0157	−0.0132	−0.0154	−0.0137	−0.0137	−0.0124	−0.0199	−0.0187
	70	−0.0232	−0.0222	−0.0222	−0.0202	−0.0182	−0.0192		
	50	−0.0276	−0.0294	−0.0274	−0.0272	−0.0252	−0.0281		

constants. Note that Eq. (1) has seven variables, only two of which are measured experimentally ($\varepsilon_{(hkl)}$ and ψ). The $\cos^2\psi$ fits provide three additional constraints, leaving two additional parameters, so the solution to Eq. (1) is not fully constrained. Therefore, an assumption must be made about either the strength or elastic constants of platinum. Platinum's bulk modulus and its pressure dependence is known from the shock equation of state data to 660 GPa,[19] as well as the elastic compliance S_{44} and its pressure dependence (but only measured to 0.25 GPa).[11] With these two parameters, we can calculate unique solutions for pressure, elastically supported differential stress (t), and the elastic constant $S_{11}-S_{12}$, which, combined with the S_{44} value, yields a measure of the elastic anisotropy.

The pressure at each compression step was calculated by referencing the hydrostatic lattice strain to the Birch-Murnaghan equation of state for platinum using $K_0 = 287$ GPa and $K_0' = 5.6$ (Table II).[19] The pressure error is determined by considering the standard deviation of the average values determined by each of the diffraction lines. The elastically supported shear stress t is calculated via Eq. (2) using $\varepsilon^{\text{amp}}_{(111)}$ and the high pressure values of S_{44} using a Birch-Murnghahan extrapolation (Fig. 4).[20] The elastic parameter $S_{11}-S_{12}[=1/(C_{11}-C_{12})]$ is calculated through Eq. (3) using $\varepsilon^{\text{amp}}_{(200)}$ and t calculated in the previous step (Table II). Finally, elastic anisotropy $2(S_{11}-S_{12})/S_{44}$ is calculated (Fig. 5). The resulting value is approximately constant with pressure, at 1.47(16) in good agreement with the ambient pressure value measured by ultrasonic methods 1.59.[21]

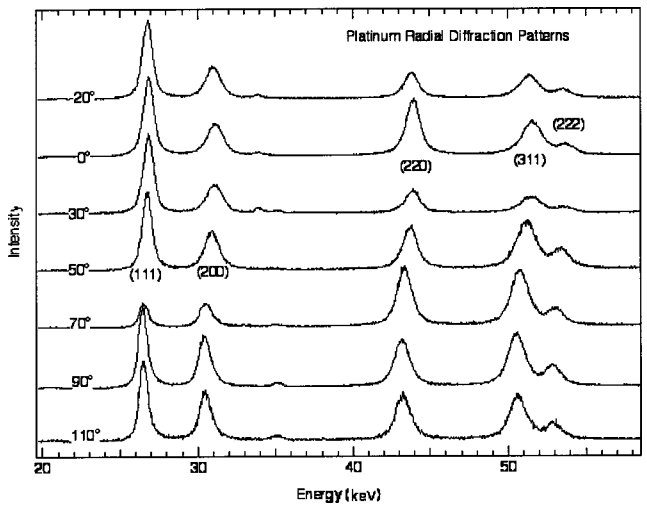

FIG. 2. The complete set of energy-dispersive diffraction patterns for platinum at 13.4(9) GPa (PtP5 in Tables I and II). Diffracted intensity is plotted as a function of energy [$2\theta = 12.000(3)$]. Each pattern is labeled by ψ angle and Pt peaks are labeled by (*hkl*) value.

DISCUSSION

Yield strength and anisotropy. The yield strength of several materials has been measured at high pressures using radial diffraction techniques. Strengths of simple metals measured via radial diffraction methods vary widely—from Au, which supports up to 0.5 GPa at 40 GPa, to Re, which supports up to 6 GPa at 40 GPa (Fig. 4). Our results for platinum, which elastically supports 2–4 GPa of shear stress between 5 and 30 GPa, suggest that it is among the stronger metals, similar to the strength of Re at high pressures. Most measurements of material strength, including these, fall significantly below estimates of the absolute ideal strength of a material[5] $G/2\pi = 10.3$ GPa for Pt. No systematic relationship between crystal structure and strength is apparent from the strength data shown in Fig. 4. For example, Pt, an fcc metal, shows similar strength to Re, an hcp metal. One method to analyze material strength in a systematic way is to normalize the strength to the (pressure dependent) shear modulus. Except for the two lowest pressure data points, t/G for platinum is approximately constant with pressure at 0.033(2). Interestingly, as a fraction of the shear modulus, Pt shows a higher strength than rhenium, whose t/G varies from 0.013 to 0.024 from 0 to 40 GPa. However, comparisons among material ''strength'' values using the radial diffraction technique is complicated by differences in material history, grain size, geometry, and strength anisotropy. Finally, these are not direct strength measurements, but rather the elastically supported differential stress at each compression; a lower bound to the actual strength.

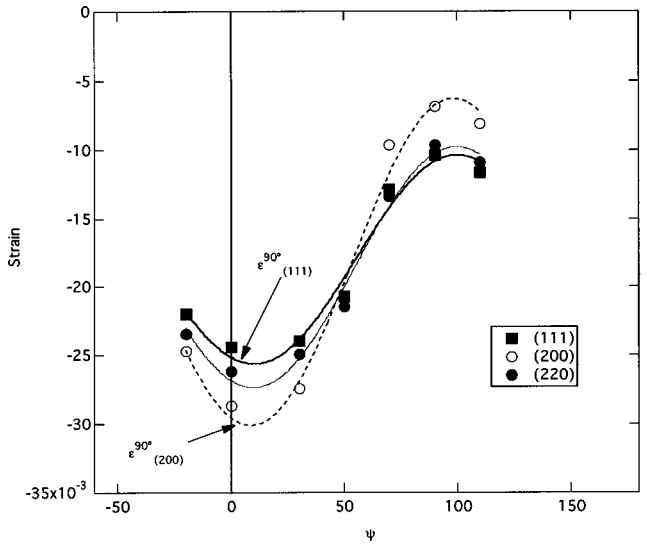

FIG. 3. Lattice strain as a function of ψ for the (111), (200), and (220) lattice plans of platinum at 13.4(9) GPa (PtP5 in Tables I and II). Black, gray, and dotted lines show $1-3\cos^2$ fits vs ψ to the (111), (220), and (200) data, respectively. Vertical line emphasizes the offset between the maximum strain recorded by the measured data (at 8.7) and the angle defining coincidence between the diamond cell and the principal stress axes (0). The error envelope surrounding the best-fit hydrostatic value of the lattice parameter is indicated by the dotted horizontal lines.

Errors in the strength measurement may derive from breakdowns in assumptions underlying Eq. (1), such as biaxial state of stress, coincidence of the diamond cell axis with the principal stress direction, and/or time-dependent stress relaxation during the experiment. All conspire to render the measured supported shear stress a lower bound on the actual maximum as discussed below. We therefore consider the differential stress measurements to be robust, especially given their duplication in two experiments with differing sample loading geometry. Although the accuracy of the analysis is limited by the uncertainties in the behavior of Pt's elastic constants under pressure, for the strength measurements, the magnitude of this error is small. Changes in the elastic anisotropy alter the difference in the lattice parameter between the (111) and (200) diffraction lines, but have little effect on the amplitude of the signal (Fig. 2). If constant strain (Voigt) conditions are assumed, the measured differential stresses will differ only slightly, well within the error bars of the determination.[17,22]

The anisotropy measurement, on the other hand, is tethered to two major assumptions: (i) the existence of constant stress conditions within the sample chamber and (ii) lattice strength isotropy. Under constant strain (Voigt) conditions, there is no Γ dependence of the lattice strain.[12] Therefore, the measured anisotropy must be considered to be a lower bound (closer to unity) on the true anisotropy value since any contribution from constant strain conditions would result in a less pronounced measurement of lattice-dependence (note that the Voigt endmember has no lattice dependence of strain). The second assumption, that each lattice plane has the same resistance to deformation, may not be true in general. For an fcc metal such as platinum, the primary slip system is $\{111\}\langle 110\rangle$.[5] Therefore, a uniaxial stress in any direction except normal to the (111) lattice plane may result in dislocation motion. However, if the $\{111\}\langle 110\rangle$ slip system is the only operable system, then an applied uniaxial stress component normal to the (111) plane will not result in any

TABLE II. Summary of platinum radial diffraction data results.

Name	(hkl)'s used in analysis	$\varepsilon_{\text{hydro}}$	$\varepsilon^{\text{amp}}_{(200)}$	$\varepsilon^{\text{amp}}_{(111)}$	Pressure (GPa)	Differential stress (GPa)	$C_{11}-C_{12}$ (GPa)	anisotropy	offset
1st set									
Pt20	111, 200, 220	−0.0162(4)[a]	−0.0061(3)	−0.0046(3)	14.7(4)	2.7(.2)	147	1.3(2)	−0.3(34)
Pt30	111 only	−0.0212(4)		−0.0053(3)	19.4(4)	3.3(.2)			2.5(31)
lowb	111, 200, 220	−0.0050(9)	−0.0063(3)	−0.0046(3)	4.2(8)	2.2(.15)	116	1.4(1)	12.8(32)
Pt10	111, 200, 220	−0.0070(1)[a]	−0.0065(3)	−0.0054(3)	5.9(1)	2.7(.4)	137	1.2(10)	16.4(05)
2nd set									
PtP1	111, 200, 220	−0.0007(3)	−0.0002(1)	−0.0002(1)	0.6(2)	0.1(.04)	149		
PtP2	111, 200, 220	−0.0034(1)	−0.0013(2)	−0.0010(2)	2.8(9)	0.5(.1)	119		
PtP3	111, 200, 220	−0.0097(8)	−0.0070(3)	−0.0047(3)	8.3(8)	2.5(.2)	116	1.49(2)	4.2(11)
PtP4	111, 200, 220	−0.0131(6)	−0.0079(3)	−0.0052(3)	11.6(6)	2.9(.15)	120	1.52(5)	8.4(14)
PtP5	111, 200, 220, 311, 222, 400, 331, 422	−0.0150(10)	−0.0079(3)	−0.0047(3)	13.4(9)	2.9(.2)	114	1.68(5)	8.7(14)
PtP6	111, 200, 220, 311, 222, 400, 331, 422	−0.0174(9)	−0.0081(3)	−0.0051(5)	15.9(9)	3.3(.3)	125	1.6(3)	3.7(21)
PtP7[b]	111, 200, 220, 311, 222, 400, 331, 422	−0.0235(13)	−0.0080(9)	−0.0051(5)	22.4(14)	3.0(.7)	139	1.6(6)	0[c]

[a] $\varepsilon_{\text{hydro}}$ from (111) line only.
[b] Two-term fits only (assume 0 offset).
[c] Assumed.

slip. Therefore, the (111) plane is expected to be the strongest plane. Since our results demonstrate the opposite, the (200) plane, not the (111) plane, shows the largest strain amplitude with ψ, the elastic anisotropy is playing a role that is at least as significant as any possible strength anisotropy. An additional crosscheck is provided by examining for lattice preferred orientation in compressed samples. No evidence of induced texturing was observed in these experiments by comparing the intensities of the Pt peaks (Fig. 2).

Composite effect. Radial diffraction experiments may provide a sensitive method to examine the stress state of each component of a composite material, to examine the mechanical behavior of microscaled composite materials, and test models of their mechanical behavior. In the experiment where both γ-$(Mg,Fe)_2SiO_4$ and platinum were loaded within the sample chamber, the hydrostatic pressure determined from platinum is systematically lower than the pressure determined from the silicate by 0.8 to 5.5 GPa across the measured pressure range. If strain continuity were to be invoked as a possible explanation for this behavior, it would predict that the material with the lower bulk modulus senses a lower pressure. This is the opposite of what is observed $[(K_{\text{spinel}}=193(3)\ \text{GPa})]$.[23] Interestingly, a similar pressure

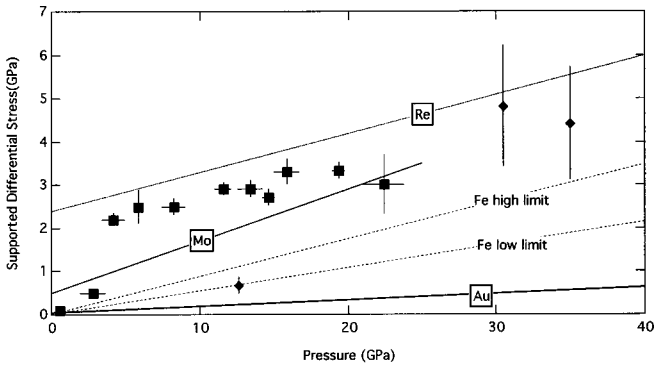

FIG. 4. Supported differential stress of metals from side diffraction experiments. Results from platinum experiments are shown as squares with error bars. Strength from Ta (Ref. 3) (diamonds), and limits on the strength of hcp Fe (Ref. 24) and Re, Mo, and Au (Refs. 15, 16) are shown as well.

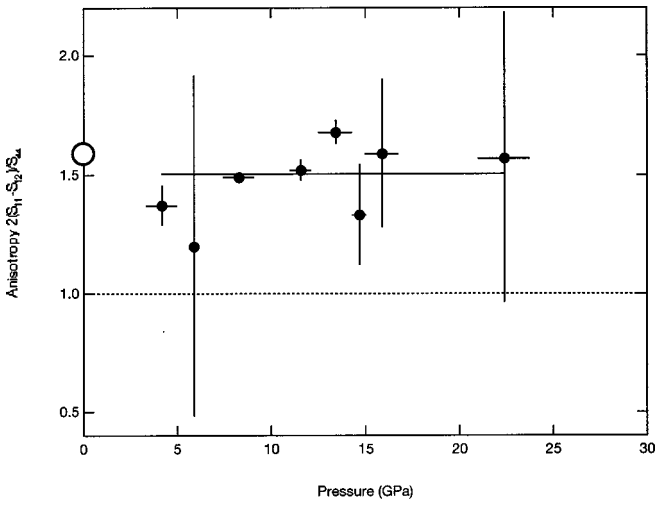

FIG. 5. Elastic anisotropy of platinum. The ambient pressure elastic anisotropy (Ref. 21) (open circle) is shown.

difference has been observed in other two-phase radial diffraction experiments.[15,16,24] As in our Pt experiments, in each of these dual systems, the material with the larger bulk modulus records lower pressures than its more compressible partner, regardless of relative strength. For the materials shown in Fig. 3, the higher bulk modulus materials Mo and Re, both record lower pressures, and Fe and γ-$(MgFe)_2SiO_4$, the more compressible materials, record higher pressures. This suggests that elastic properties as well as material strength control the mechanical behavior in the diamond cell.

In composite systems, both elastic properties and geometry play a role in determining how much pressure each phase sustains. If, for example, the Pt and γ-$(Mg,Fe)_2SiO_4$ are arranged so that they contact in the diamond cell axis (''sandwich geometry''), the maximum stress σ_1 (in the direction of the axial load of the diamonds) is the same for both platinum and γ-$(Mg,Fe)_2SiO_4$. However, this assumption makes the results from the two materials even less compatible. The values of σ_1, determined by $\sigma_1 = P + 2/3t$, are 4 to 10 GPa higher in the γ-$(Mg,Fe)_2SiO_4$ than in Pt. However, the data are consistent if the radial component of the stress experienced by Pt and γ-$(Mg,Fe)_2SiO_4$ are equal. Information about the geometric relationship between the two materials was lost upon removal of the sample.

The difference in pressure can be explained by recognizing that under nonhydrostatic conditions, significant pressure gradients exist within the diamond anvil cell sample chamber.[25] An alternative method to measure yield strength of materials at high pressures takes advantage of these pressure gradients to calculate $\sigma_y = h(dP/dr)$, where σ_y is the yield strength, h is the sample thickness, P is the pressure measured by ruby fluorescence, and r is the radial distance from the center of the diamond-anvil cell axis.[25] Although h was not directly measured in this experiment, typical sample thicknesses at these pressures range from 10–20 μm. It is possible that plastic deformation during the experiment caused rearrangement of platinum and γ-$(Mg,Fe)_2SiO_4$ so that they were laterally displaced with respect to the axial diamond cell load by 5–10 μm. Using the pressure difference between γ-$(Mg,Fe)_2SiO_4$ and platinum, differential stresses calculated via the pressure gradient method (above) range from 1.5–4.5 GPa at the lowest pressure to 5.5–15.5 GPa at the highest pressure. These numbers are a bit larger, but still consistent with the yield strength measurements obtained by the lattice strain theory.

Since the sample geometry was not controlled in this experiment, a quantitative analysis of the composite effect is precluded. The angular offset between the diamond cell and the principal stress directions (Table II and Fig. 3) recorded in these experiments testify to a more complex geometry within the sample chamber than either side-by-side or ''sandwich.'' Modeling of the stress environment in the diamond cell sample chamber and controlled-geometry radial diffraction experiments are currently in progress to fully explain this behavior quantitatively.

Transient creep. To investigate time-dependent relaxation of platinum under nonhydrostatic pressures, the (111) and (200) lattice parameters of experiment PtP3 (Table I) were

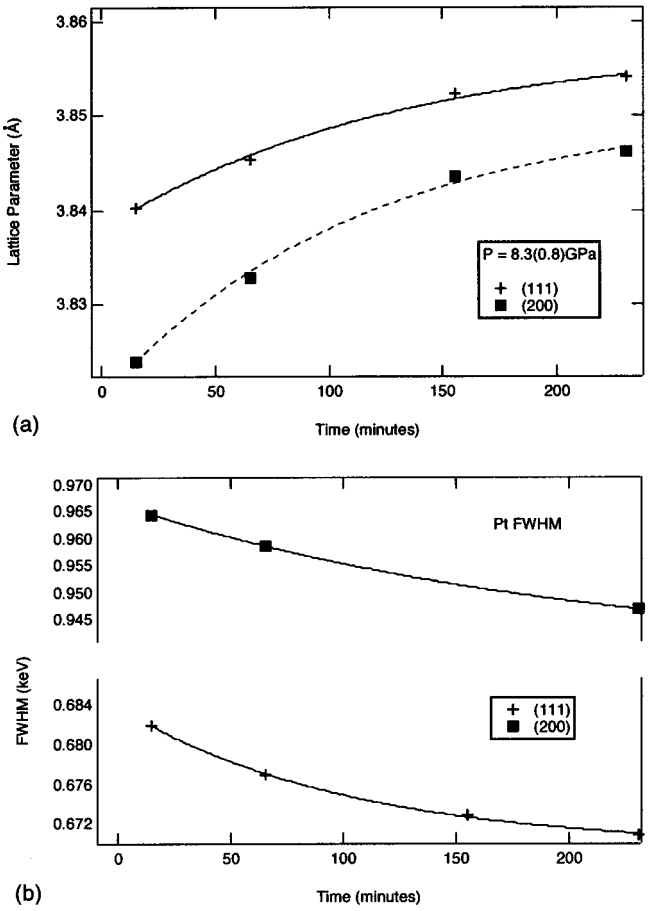

FIG. 6. Time variation of (a) lattice parameter and (b) diffraction peak widths of platinum under nonhydrostatic stress, at $\psi = 0°$ (maximum stress orientation).

monitored at the maximum stress direction over the course of 4 h. The resulting observations are (a) a systematic increase with time of the lattice parameter of both the (111) and (200) lines and (b) a trend toward convergence of the (111) and (200) diffraction lines [Fig. 6(a)]. Both observations signify a time-dependent relaxation of the differential stress. Plastic processes are not directly measured in these experiments; rather, we are measuring the elastic response to a decrease in differential stress accompanied by plastic relaxation processes. This can be caused either by plastic creep of the platinum sample itself, or by relaxation of the beryllium gasket surrounding the sample. Two lines of evidence suggest the former: (a) platinum's diffraction peak width, an indicator of microscopic stresses also decreases over this time period with the same characteristic relaxation time of about ~120 min [Fig. 6(b)], indicating a change of the microscopic behavior of platinum and that (b) similar time-dependent behavior was not observed for the γ-$(Mg,Fe)_2SiO_4$ sample, an even stronger material,[9] despite the use of similar Be gasket material.

The observation of time-dependent behavior in Pt under nonhydrostatic stress is remarkably similar to behavior observed in a separate set of experiments reported elsewhere in which platinum was laser heated to ~1200(300) K within a steel gasket [Fig. 7(a) and 7(b)].[9] In the laser heating experiment, the same observations were made: (111) and (200)

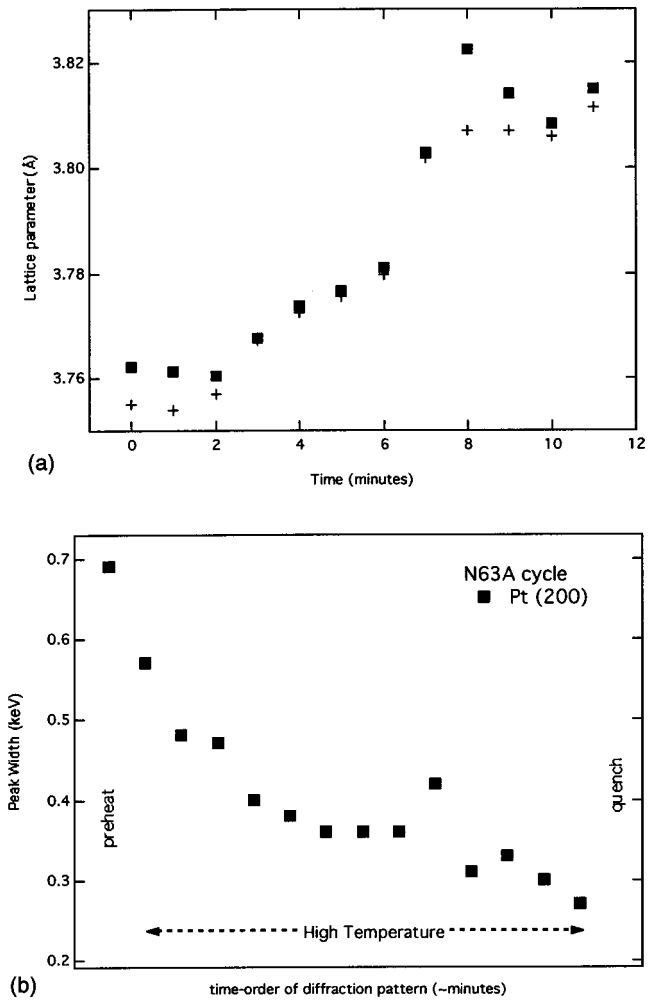

FIG. 7. Time variation of the lattice parameter (a) and diffraction peak widths (b) of platinum during laser heating at $\psi \sim 84°$ (diamond cell axis is close to the minimum stress orientation). The temperatures are fluctuating during this experiment, and the x-ray beam is capturing x-ray intensity originating over large temperature gradients. The average temperature in these experiments is about 1200 K.

strains (lattice parameters) show time-dependent relaxation, their values converge, and their diffraction peak widths decrease with time during laser heating all within the same timescale (~min). For both high- and low-temperature processes, the magnitudes of the deviatoric stress (~GPa) and the strain relaxation (0.5%) were the same; only the time scale differed (two orders of magnitude faster for the high-temperature processes), leading to an average strain rate of $\sim 8 \times 10^{-5}$ s^{-1} for Pt at 1200 K and $\sim 7 \times 10^{-7}$ s^{-1} at 300 K.

An effective viscosity for creep processes under nonhydrostatic stresses can be calculated using $\eta = \sigma_s / (d\varepsilon/dt)$ where η is the dynamic viscosity, σ_s is the supported shear stress, and $d\varepsilon/dt$ is the observed strain rate.[26] The resulting viscosity measured for platinum in the high- and low-temperature experiments are 10^{13} Pa s at 1200(300) K and 10^{15} Pa s at 300 K. (For comparison, viscosity of glacial ice is $\sim 10^{13}$ Pa s.) Unfortunately, the lack of room temperature creep data on platinum precludes a direct comparison with other techniques. However, creep measurements for pure metals such as Ni and Cu (Ref. 27) show similar values. For example, copper creep experiments measure 0.102% elongation resulting from 6000 h under 54.6 MPa of applied stress at 422 K. This implies a viscosity of $\sim 10^{15}$ Ps s, similar to our inferred room temperature Pt viscosity. Similar viscosities are inferred from experiments on cold-worked pure Ni.[27]

Damping experiments indicate that platinum's relaxation mechanism changes from dislocation glide at low temperature to diffusion-aided recrystallization and grain growth at high temperatures.[27] Therefore, the two measured data points cannot be used to infer an activation energy for a single process. Although these results are preliminary, they raise the prospect of quantitative viscosity measurements in the diamond-anvil cell. These measurements are especially important for the study of planetary interiors, where relevant viscosities range from 10^{19}–10^{21} Pa s. In this case, we were able to measure viscosities as high as 10^{15} Pa s only because we were employing such large (~GPa) nonhydrostatic stresses. Of course, the shear stresses experienced in planetary interiors are orders of magnitude smaller. This requires being mindful of scaling issues when trying to extrapolate results from diamond-cell scale experiments to planetary-scale applications.

ACKNOWLEDGMENTS

We thank J. Hu for experimental assistance at Beamline X17C at NSLS. This work was supported by the NSF and the David & Lucille Packard Foundation. A.K. was supported by the Lamont Doherty Earth Observatory for part of this research. Research was carried out (in part) at the National Synchrotron Light Source, Brookhaven National Laboratory, which is supported by the U.S. Department of Energy, Division of Materials Sciences and Division of Chemical Sciences, under Contract No. DE-AC02-98CH10886.

*Present address: Dept. of Earth and Space Sciences and Institute of Geophysics and Planetary Physics, UCLA, Los Angeles, CA 90095-1567.

[1] S. Karato, Phys. Earth Planet. Inter. **24**, 1 (1981).
[2] S. Karato and P. Wu, Science **260**, 771 (1993).
[3] S. T. Weir, J. Akella, C. Ruddle, T. Goodwin, and L. Hsiung, Phys. Rev. B **58**, 11 258 (1998).
[4] H. J. Frost and M. F. Ashby, *Deformation-mechanism Maps: The Plasticity and Creep of Metals and Ceramics*, 1st ed. (Pergamon Press, Oxford, 1982); S. Karato and H. A. Spetzler, Rev. Geophys. **28**, 399 (1990).
[5] G. E. Dieter, *Mechanical Metallurgy*, 3rd ed. (McGraw-Hill, New York, 1986).
[6] Gene Simmons and H. Wang, *Single Crystal Elastic Constants and Calculated Aggregate Properties: A Handbook*, 2nd ed. (The M.I.T. Press, Cambridge, MA, 1971).
[7] Gerd Steinle-Neumann, Lars Stixrude, R. E. Cohen, and O. Gulseren, Nature (London) **413**, 57 (2001).

[8] D. Andrault, G. Fiquet, J. P. Itie, P. Richet, P. Gillet, D. Hausermann, and M. Hanfland, Eur. J. Mineral. **10**, 931 (1998); A. Dewaele, G. Fiquet, D. Andrault, and D. Hausermann, J. Geophys. Res., [Solid Earth] **105**, 2869 (2000); S. H. Shim, T. S. Duffy, and G. Y. Shen, *ibid.* **105**, 25 955 (2000).
[9] A. Kavner and T. S. Duffy, J. Appl. Phys. **89**, 1907 (2001).
[10] Y. Higo, T. Inoue, T. Irifune, and H. Yurimoto, Geophys. Res. Lett. **28**, 3505 (2001); S. H. Shim, T. S. Duffy, and G. Y. Shen, Nature (London) **411**, 571 (2001).
[11] S. N. Biswas, M. J. Muringer, and C. A. ten Seldam, Phys. Solid State **141**, 361 (1994).
[12] A. K. Singh, J. Appl. Phys. **73**, 4278 (1993).
[13] A. K. Singh, C. Balasingh, H. K. Mao, R. J. Hemley, and J. F. Shu, J. Appl. Phys. **83**, 7567 (1998).
[14] A. K. Singh and T. Kenichi, J. Appl. Phys. **83**, 7567 (1998).
[15] T. S. Duffy, G. Y. Shen, D. L. Heinz, J. F. Shu, Y. Z. Ma, H. K. Mao, R. J. Hemley, and A. K. Singh, Phys. Rev. B **60**, 15 063 (1999).
[16] T. S. Duffy, G. Y. Shen, J. F. Shu, H. K. Mao, R. J. Hemley, and A. K. Singh, J. Appl. Phys. **86**, 6729 (1999).
[17] A. Kavner and T. S. Duffy, Geophys. Res. Lett. **28**, 2691 (2001).
[18] S. Merkel, H. R. Wenk, J. F. Shu, G. Y. Shen, P. Gillet, H. K. Mao, and R. J. Hemley, J. Geophys. Res., [Solid Earth] **107**, B11 (2002); S. Merkel, A. P. Jephcoat, J. Shu, H. K. Mao, P. Gillet, and R. J. Hemley, Phys. Chem. Miner. **29**, 1 (2002).
[19] N. C. Holmes, J. A. Moriarty, G. R. Gathers, and W. J. Nellis, J. Appl. Phys. **66**, 2962 (1989).
[20] Francis Birch, J. Geophys. Res. **83**, 1257 (1978).
[21] R. E. Macfarlane, J. A. Rayne, and C. K. Jones, Phys. Lett. **18**, 91 (1965).
[22] A. Kavner, Earth Planet. Sci. Lett. (to be published).
[23] S. V. Sinogeikin, J. D. Bass, A. Kavner, and R. Jeanloz, Geophys. Res. Lett. **24**, 3265 (1997).
[24] R. J. Hemley, H. K. Mao, G. Y. Shen, J. Badro, P. Gillet, M. Hanfland, and D. Hausermann, Science **276**, 1242 (1997).
[25] C. Meade and R. Jeanloz, J. Geophys. Res. **93**, 3261 (1988); **93**, 3270 (1988); Nature (London) **348**, 533 (1990).
[26] Giorgio Ranalli, *Rheology of the Earth*, 2nd ed. (Chapman and Hall, London, 1995).
[27] *Smithells Metals Reference Book*, 7th ed., edited by E. A. Brandes and G. B. Brook (Butterworth and Heinemann, Oxford, 1992).